

Coordination of DC power flow controllers and AC/DC converters on optimising the delivery of wind power

Sheng Wang¹ ✉, Jingli Guo², Chuanyue Li¹, Senthoran Balasubramaniam¹, Rui Zheng¹, Jun Liang¹

¹School of Engineering, Cardiff University, CF24 3AA, Cardiff, UK

²School of Electrical Engineering, Xi'an Jiaotong University, 710049, Xi'an, People's Republic of China

✉ E-mail: WangS9@cf.ac.uk

ISSN 1752-1416

Received on 30th September 2015

Revised on 9th December 2015

Accepted on 8th January 2016

doi: 10.1049/iet-rpg.2015.0452

www.ietdl.org

Abstract: The generation of offshore wind power is less predictable. This can cause the overload of offshore DC transmission system and thus requires the curtailment of wind power. To reduce the amount of wind power curtailment, a method of optimising DC power flow using DC power flow controller (DC-PFC) is proposed. The analytical expression of coordinating DC-PFCs and converters in controlling the power flow of the DC system has been created. Method has been developed to optimise the power flow of DC grids within which control setting changes automatically in different wind conditions to reduce both the power curtailment and power losses. The proposed method has been demonstrated and validated on a 9-port DC system. It is concluded that both the curtailment of wind power and power losses are effectively reduced by inserting DC-PFCs into DC grids.

1 Introduction

The increasing capacity of offshore windfarms drives the development of reliable and economical offshore corridors for power transmission. Various manufacturers and academia have addressed on this challenge while agreeable conclusion has been drawn on building a VSC based offshore DC network [1–3]. Practice of using point to point HVDC link for offshore power transmission includes the Dolwin1 [4], Borwin1 [5] and Nanhui [6]. These links could possibly be integrated to form a meshed offshore DC supergrid in the upcoming decades. Such a DC grid will then have a meshed topology which provides multiple paths for power flow and thus enhances the reliability of DC system [7]. Furthermore, the controllability of AC/DC converters over the converter power flow makes possible the delivery of wind energy across the network more flexible. However, power flow within the meshed DC branches remains uncontrollable and determined by the differential voltage across branches. This raises the potential risk of overloading of certain branch (especially in events of fluctuating power source connected) while the other branches may even still be underutilised. Curtailment of wind power may thus be required in such an event of overloading, whilst the cost of reducing wind power generation is quite undesirable due to its positive environmental characteristics. There is then greater incentive to find an alternative way to optimise DC power flow thus to avoid overloading and reduce the curtailment of wind power. A few studies have been proposed on developing DC power flow controllers (DC-PFCs) which can be inserted into branches to control the branch power and avoid overloading of certain branch. These devices act as either voltage sources [8–10] or variable resistors (VRs) [11] to regulate the branch power. The effectiveness of using DC-PFCs has been well demonstrated at the local control level in the above literatures. Discussion stays quite open on its application and coordination control within AC/DC converters. This paper intends to make a contribution of coordinating converters and DC-PFCs for optimising the delivery of wind power and reducing both the power curtailment (caused by overloading) and the inevitable resistive line losses.

The rest of this paper is arranged as follows. Section 2 introduces the control strategies of DC Grid. The control of different types of

DC devices is also presented. Section 3 describes the expression for regulating DC power flow. The impact of dispatched control orders (for both DC-PFCs and converters) on power flow is analysed in a quantitative way. Section 4 details the algorithm of re-dispatching control orders for power flow optimisation. Section 5 presents the case studies followed by the conclusions drawn in Section 6.

2 Control strategies of DC grid

The control of a DC grid has been much discussed [12–16] over recent years though mostly have excluded DC-PFCs. It broadly falls into two control layers: decentralised primary control and centralised secondary control. In this paper, the discussion of controlling DC-PFCs is also merged into both control layers. Fig. 1 shows the structure of such a hierarchical control system.

The centralised secondary control is conducted within a grid dispatch centre (GDC), where local measurements of both AC/DC converters and DC-PFCs are periodically updated via telecommunications to a system monitor. The GDC will evaluate the operating status of the entire DC grid by estimating branch resistances and power flow of system. It will then be economic benefit to update new control orders (using the obtained information), often for purposes such as avoiding power curtailment, reducing resistive losses and optimising system voltages. These control orders will periodically be fed back to each individual DC component for primary control.

The primary control then acts to coordinate controllable DC devices mainly on regulating DC voltages and converter power. It allows the system operating safely and in a predicable manner even in events of telecommunication failed. One underlying concept for primary control is the most common, acknowledged as the DC voltage droop control within which AC/DC converters connected to strong AC grid share of the responsibility of regulating DC voltages. However, those connected to wind farms and island loads have to be in a form of integration of power control mode in order to maintain the AC side frequency within an acceptable range. Meanwhile, the DC-PFC that have been integrated always intend to control the power or current flowing

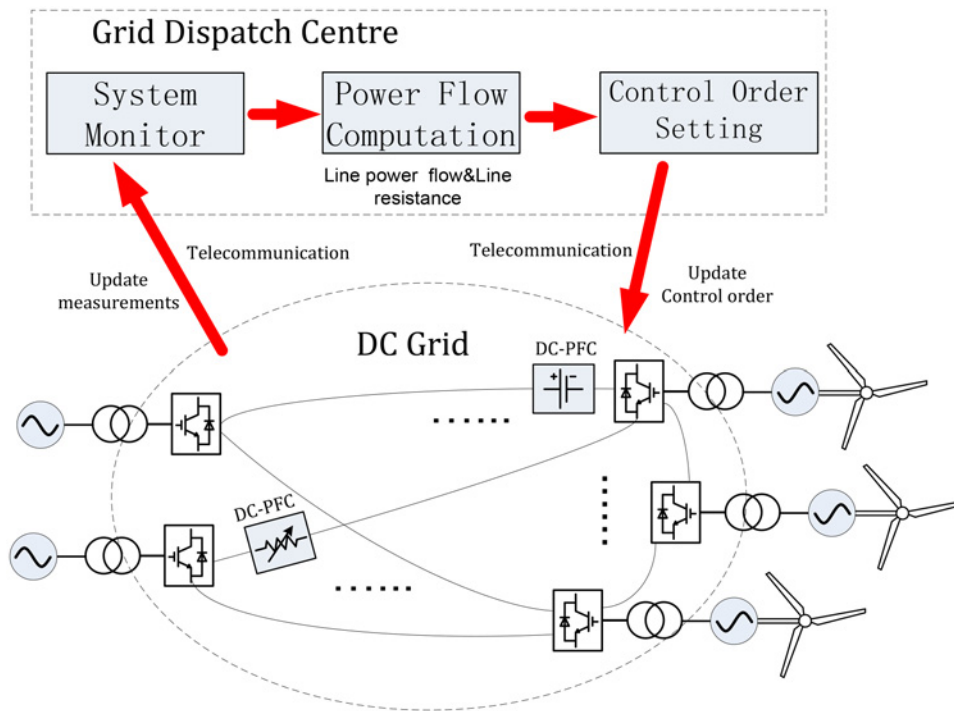


Fig. 1 Hierarchical control system of a DC grid with a DC-PFC integrated

through certain branches thus to avoid overloading or to optimise the power flow within the DC system. Note that a DC-PFC may control the power through the local branch whilst is not necessary. In state-steady, a DC-PFC is also capable to control power flowing through a remote branch via low bandwidth telecommunications.

2.1 Control of DC-PFCs

A DC-PFC targets for regulating branch power or current by either inserting a controllable voltage source (CVS) or a VR. Early work on CVS (Fig. 2a) has proposed the use of two six-pulse thyristor converters connected in a dual-converter configuration, where voltage can be injected by exchanging power with the AC system. Analogue is the use of a combination of an IGBT based AC/DC converter and a DC/DC converter (Fig. 2b). Both devices are able to control the power flow through certain branches (P_{BR}) by adjusting the injected voltages (U_{INT}). Note that a bit change on

the injected voltage (e.g. 5% of system voltage rate) is usually enough to have a marked effect on power flow since the devices are connected in series with DC branches. This in turn indicates DC-PFCs will have much smaller rate of voltage and power, compared with the AC/DC converters that interconnect AC systems with DC grids. A CVS is thus compatible for flexibly controlling power in a cost effective way. Views regarding to its disadvantage could be the disproportionately sized auxiliary transformer, which has to be rated at system level to withstand the AC voltage. Researchers thus propose an alternative power flow controller [17–19] (see Fig. 2c) in order to avoid using such an auxiliary transformer. This type of controller has two full-bridge DC/DC converters while each is connected in series with one of the DC branches (connected to the same AC/DC converter). A mean DC voltage will then be inserted into each DC line to change the power flowing through the DC/DC converters and thus controls the power of DC branches.

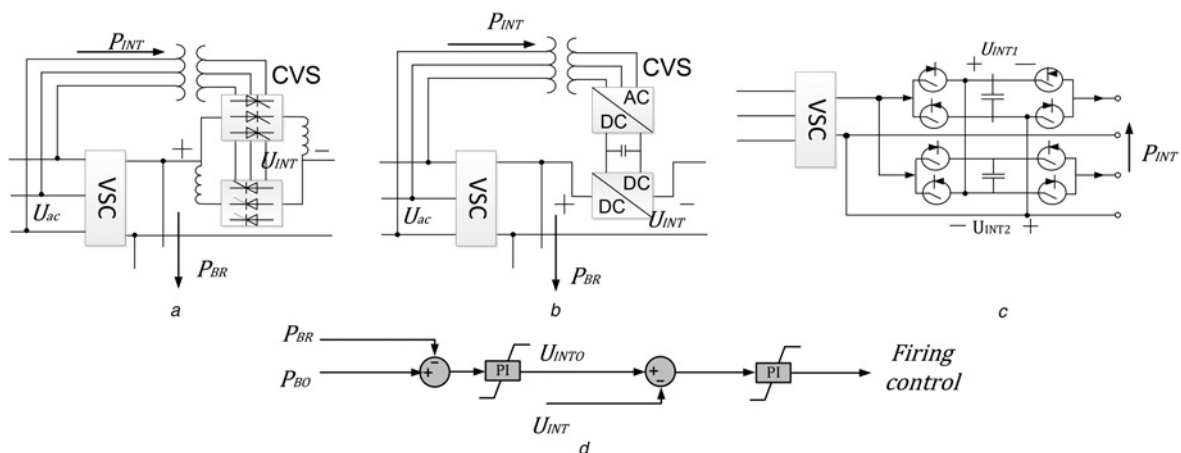


Fig. 2 Structures of CVSs

- a Thyristor based power-flow controller
- b IGBT based power-flow controller
- c Alternative power flow controller
- d Control scheme of a CVS

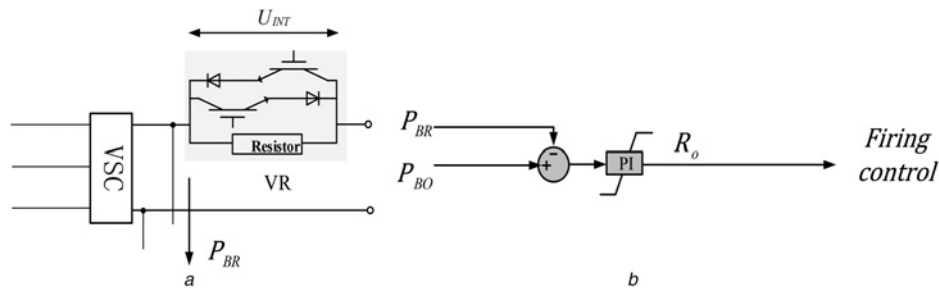


Fig. 3 Variable resistor (VR)

a Structures of a VR
b control scheme of a VR

The control schemes of various types of CVS have difference in firing control whilst have much similarity in upper control loop. An example is given in Fig. 2d. A GDC will send power order (P_{BO}) via telecommunications to each CVS. The control of CVS follows the order and generates an internal voltage reference (U_{INTO}) to lower level for firing control. The power flow through the controlled branch (P_{BR}) will then be equal to P_{BO} in steady-state.

A few studies have also addressed on the concept of using VR to control branch power. An example is given in Fig. 3a where a resistor is in parallel with a pair of IGBTs and diodes that are connected in a bidirectional way. IGBTs operate to adjust the effective resistance inserted to the circuits regarding to the resistance reference (R_o) (Fig. 3b). Branch power can thus be controlled whilst the cost of additional losses on the resistor makes it less attractive.

2.2 Control dynamics of DC-PFCs

The control dynamics of DC-PFCs are important research topics. Some work has been done in [10, 11, 18, 20, 21] to address on the control dynamics of different types of DC-PFCs. These DC-PFCs can control a power through one DC branch to a certain level within several hundred milliseconds due to the operating of fast switching devices (i.e. IGBTs or thyristors). The fast switching devices in turn will generate small harmonics in transient. However, as the size of DC-PFCs is much smaller than the system rating, these harmonics are ignorable and will have little impact on the dynamics of overall voltages and power of HVDC-VSCs [21]. The design of control orders of both DC-PFCs and HVDC-VSCs is also very unlike to take into account the dynamic interactions between DC-PFC and HVDC-VSCs. As previously mentioned, the coordinating control of DC-PFC and HVDC-VSCs aims at controlling the DC system power flow in a relatively long term (compared with several hundred milliseconds), for purpose such as to avoid overloading or to optimise the power flow within the DC system. This paper thus focuses on optimising

the DC power delivery based on the static analysis of power flow control.

2.3 Control of AC/DC converters

The market of using modular multi-level converter (MMC) in HVDC network keeps growing rapidly. Each valve of an MMC (see Fig. 4a) has hundreds of sub-modules connected as 'chain links' where the switching of each IGBT is individually controlled to produce a sinusoidal voltage.

With the DC voltage control, the local controller (see Fig. 4b) of each MMC is assigned with a DC voltage/power droop which allows the MMC to regulate its own DC voltage by adjusting the converter power. The droop characteristic is mathematically given by

$$k \times (U_{CO} - U_{CM}) = (P_{CO} - P_{CM}) \quad (1)$$

where U_{CO} and P_{CO} are the control orders of voltage and power; U_{CM} and P_{CM} are the measurements of converter DC voltage and power. The DC power/voltage droop k reflects the sensitivity of power deviation to DC voltage change.

Well dispatched control orders would locate the actual operating point (OP_{CM}) (Fig. 4c) very close to the desirable operating point OP_{CO} (where U_{CO} is equal to U_{CM} and P_{CM} is equal to P_{CO}). However, in practical, the control accuracy of current and voltage is influenced by the following items [22]:

- Measurement errors of DC voltage/DC current transducers.
- Wrong computation of DC network resistance of GDC.
- Telecommunication loss of GDC and local converters during change of load/generation conditions.
- Instantaneous power disturbance within a DC grid.

Therefore, the actual operating point OP_M could drift along the droop line away from the desirable operating point. Moreover, the integration of DC-PFCs will apparently have an impact on the

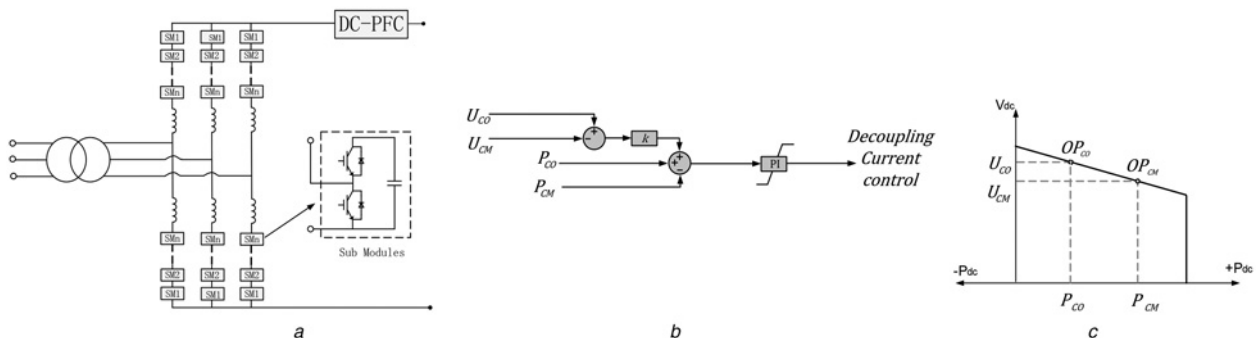


Fig. 4 Modular multi-level converter (MMC)

a Structure of MMC
b Control scheme of a MMC
c Voltage/power characteristic

converter power. For sure DC-PFCs are mean to accurately control some of the branch power while this could add up to the possibility of converter operating points drifting away from the desirable operation points. The GDC will thus also have the responsibility of re-dispatching control orders to optimise the converter operating. The coordination of converter control and DC-PFC control on power flow should then be addressed. The impact of re-dispatching control orders on system operating (e.g. power flow, voltage) should be represented in a more ‘quantified’ way. This is discussed in Section 3.

3 Impact of coordinating control of AC/DC converters and DC-PFCs on DC power flow

The DC power flow expression for a DC grid without any DC-PFCs is similar to the matrix formulation of AC power flow, which is given as

$$\mathbf{P}_{CM} = \mathbf{U}_{CM} \otimes \mathbf{G} \mathbf{U}_{CM} \quad (2)$$

where \otimes is the entry-wise matrix multiplication operator; \mathbf{P}_{CM} and \mathbf{U}_{CM} are vectors representing the converter power and DC voltage

$$\begin{aligned} \mathbf{P}_{CM} &= [P_{CM,1} \cdots P_{CM,i} \cdots P_{CM,m}]^T \\ \mathbf{U}_{CM} &= [U_{CM,1} \cdots U_{CM,i} \cdots U_{CM,m}]^T \end{aligned} \quad (3)$$

Note that a DC transmission system has ignorable reactance and thus represented by conductance matrix \mathbf{G} in (2). Moreover, there may be ride-through DC buses which are not connected to any converter. These ride-through DC buses can mathematically be considered as converter-connected but have no power exchange with the AC system.

Modification will apparently be needed if DC-PFCs are integrated. Fig. 5a shows an example where a DC grid composed of m converters and n DC-PFCs.

Small differential voltage ($U_{INT,j}$) has been induced by DC-PFC $_j$. The locally internal power transferring of the DC-PFC ($P_{INT,j}$) is

given as

$$P_{INT,j} = U_{INT,j} \times (U_{CM,j} - U_{CM,2}) \times G_{2j} \quad (4)$$

where $U_{CM,2}$ is the converter voltage for VSC $_2$. The installation of a DC-PFC equivalently creates a new node (within the DC system) which provides an additional dimension for controlling power flow. The G_{2j} is then the conductance between the created node and VSC $_2$. The obtained $P_{INT,j}$ can either represent the power exchange of a CVS or the power dissipation of a VR. Therefore, by merging n sets of power flow expression for DC-PFCs (i.e. n sets of (4)) into the original power flow formulation (i.e. (2)), a general expression for the power flow in a m converters DC grid with n DC-PFCs is obtained as

$$\begin{bmatrix} \mathbf{P}_{CM} \\ \mathbf{P}_{INT} \end{bmatrix} = \begin{bmatrix} \mathbf{U}_{CM} \\ \mathbf{U}_{INT} \end{bmatrix} \otimes \begin{bmatrix} \mathbf{G} & \mathbf{G}_c^T \\ \mathbf{G}_c & 0 \end{bmatrix} \begin{bmatrix} \mathbf{U}_{CM} \\ \mathbf{U}_{INT} \end{bmatrix} \quad (5)$$

where \mathbf{P}_{INT} , \mathbf{U}_{INT} are vectors representing the local power transferring of DC-PFCs and the induced differential voltages, \mathbf{G}_c is an $n - by - m$ conductance matrix. Non-zero elements in \mathbf{G}_c represent the conductance of branches where DC-PFCs are located (e.g. G_{2j}).

The number of variables in (5) will further increase if the type of DC-PFC shown in Fig. 2c is in use. This is because adding one of such a DC-PFC will create two extra nodes (j and g) as shown in Fig. 5b. This DC-PFC can then be considered as two equivalent CVSs whilst are electrical coupled. The internal power exchange of two equivalent CVSs has a relationship of $P_{INT,g} = -P_{INT,j}$. The (5) stays the same whilst with an increase in variables.

Equation (5) mathematically shows the impact of converter voltage and induced differential voltage on converter power and local power transferring of DC-PFC. The influence of control on power flow is not reflected. It then becomes more interesting to address on the impact of changing control orders on system power flow.

As previously mentioned the control orders given by the GDC includes both the orders for MMCs (U_{CO} , P_{CO} and k) and those for DC-PFCs (P_{BO}). In steady-state, the operating points of MMCs will follow the droop characteristics (1) and the controlled branch

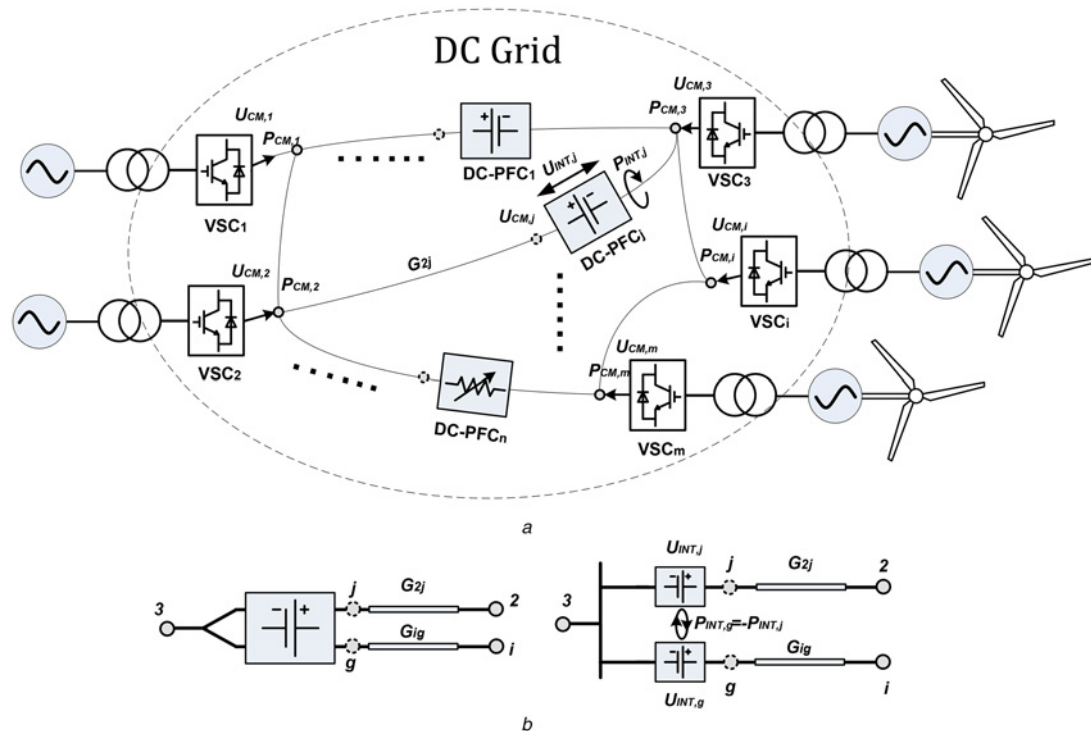


Fig. 5 DC grid integrated with m AC/DC converters and n DC-PFCs

power will equal to the ordered power for DC-PFCs (i.e. $P_{BR} = P_{BO}$). Therefore, the relationship amongst a set of power flow and control orders is given in a matrix form

$$\begin{cases} P_{CM} = P_{CO} + \mathit{diag}(k) \times (U_{BO} - U_{CM}) \\ P_{BR} = P_{BO} \end{cases} \quad (6)$$

where, $\mathit{diag}(k)$ are diagonal matrix representing the droops.

To link with the DC power flow described by (5), assuming the internal power of a DC-PFC and the controlled branch power (or branch power order) has a ratio of ε

$$\varepsilon = P_{INT,j}/P_{BR,j} = P_{INT,j}/P_{BO,j} \quad (7)$$

Equation (6) can then be re-written into small-signal form

$$\begin{cases} \Delta P_{CM} = \Delta P_{CO} + \mathit{diag}(k) \times (\Delta U_{CO} - \Delta U_{CM}) \\ \Delta P_{INT} = \mathit{diag}(\varepsilon)^{(t)} \times \Delta P_{BO} \end{cases} \quad (8)$$

Note that changes in power reference or power of DCPFC will cause the change of ratio between P_{INT} and P_{BR} . Therefore, similar to any Jacobean matrix, the elements in $\mathit{diag}(\varepsilon)^{(t)}$ need to be updated as below

$$\varepsilon^{(t+1)} = \varepsilon^{(t)} + \frac{d\varepsilon}{dP_{INT}} \Delta P_{INT,j} + \frac{d\varepsilon}{dP_{BR}} \Delta P_{BR,j} \quad (9)$$

We can also obtain the small-signal matrix for (5) by differentiation

$$\begin{bmatrix} \Delta P_{CM} \\ \Delta P_{INT} \end{bmatrix} = \begin{bmatrix} J_{m/m} & J_{m/n} \\ J_{n/m} & J_{n/n} \end{bmatrix} \begin{bmatrix} \Delta U_{CM} \\ \Delta U_{INT} \end{bmatrix} \quad (10)$$

where $J_{m/m}$, $J_{m/n}$, $J_{n/m}$ and $J_{n/n}$ form the Jacobian matrix reflecting the power deviation respecting to the voltage change of converters and DC-PFCs. Conclusively by combining (8) and (10) gives (see (11))

where $\mathit{diag}(1)$ is the identity matrix. Equation (11) shows the impact of changing control orders on the converter power and internal

power transfer of DC-PFCs. Similarly, the impact of changing control orders on system DC voltages can also be derived as (12) (see (12))

Both (11) and (12) clearly show the quantised impact of changing control orders on system operation. The linearised relationship amongst control orders, DC power and DC voltage can be used to solve power control problems. For example, the GDC would like to change the power flow through converters by ΔP_{CM} while have a change of ΔU_{CM} in DC voltages. By solving the inverse function of (11) and (12), the required amount of change in control orders can be evaluated.

Moreover, this paper also takes a further step to use this conclusion for solving non-linear optimisation problems. Details are presented in Section 4.

4 Optimisation of DC power flow

4.1 Objective function

This study specifically addresses on the optimisation of wind power delivery since it is very likely that a DC grid will be integrated with remote offshore wind farms. It is thus reasonable to have an objective function of maximising the wind power delivery to the onshore system, which indicates to:

- First, reduce the curtailment of wind power due to overload of DC branch.
- Second, reduce the resistive line losses.

This can be expressed by

$$\text{Max} \left\{ \sum_1^r P_{inv,i} \right\} = \text{Max} \left\{ \sum_1^g (P_{wf,f} - P_{cur,f}) - \sum_1^v P_{loss} - \sum_1^y P_{INT,VR} \right\} \quad (13)$$

where $\sum_1^r P_{inv,i}$ represents the total power received by onshore

$$\begin{cases} \begin{bmatrix} \Delta P_{CM} \\ \Delta P_{INT} \end{bmatrix} = \begin{bmatrix} \frac{\partial P_{CM}}{\partial P_{CO}} & \frac{\partial P_{CM}}{\partial P_{BO}} \\ \frac{\partial P_{INT}}{\partial P_{CO}} & \frac{\partial P_{INT}}{\partial P_{BO}} \end{bmatrix} \begin{bmatrix} \Delta P_{CO} \\ \Delta P_{BO} \end{bmatrix} + \begin{bmatrix} \frac{\partial P_{CM}}{\partial U_{CO}} & \mathbf{0} \\ \frac{\partial P_{INT}}{\partial U_{CO}} & \mathbf{0} \end{bmatrix} \begin{bmatrix} \Delta U_{CO} \\ \mathbf{0} \end{bmatrix} \\ \begin{bmatrix} \frac{\partial P_{CM}}{\partial P_{CO}} & \frac{\partial P_{CM}}{\partial P_{BO}} \\ \frac{\partial P_{INT}}{\partial P_{CO}} & \frac{\partial P_{INT}}{\partial P_{BO}} \end{bmatrix} = \left\{ \begin{bmatrix} \mathit{diag}(k) & \mathbf{0} \\ \mathbf{0} & \mathbf{0} \end{bmatrix} \begin{bmatrix} J_{m/m} & J_{m/n} \\ J_{n/m} & J_{n/n} \end{bmatrix}^{-1} \right\}^{-1} \times \begin{bmatrix} \mathit{diag}(1) & \mathbf{0} \\ \mathbf{0} & \mathit{diag}(\varepsilon)^{(t)} \end{bmatrix} \\ \begin{bmatrix} \frac{\partial P_{CM}}{\partial U_{CO}} & \mathbf{0} \\ \frac{\partial P_{INT}}{\partial U_{CO}} & \mathbf{0} \end{bmatrix} = \left\{ \begin{bmatrix} J_{m/m} & J_{m/n} \\ J_{n/m} & J_{n/n} \end{bmatrix}^{-1} + \begin{bmatrix} \mathit{diag}(k) & \mathbf{0} \\ \mathbf{0} & \mathbf{0} \end{bmatrix} \right\}^{-1} \times \begin{bmatrix} \mathit{diag}(1) & \mathbf{0} \\ \mathbf{0} & \mathit{diag}(\varepsilon)^{(t)} \end{bmatrix} \end{cases} \quad (11)$$

$$\begin{cases} \begin{bmatrix} \Delta U_{CM} \\ \Delta U_{INT} \end{bmatrix} = \begin{bmatrix} \frac{\partial U_{CM}}{\partial P_{CO}} & \frac{\partial U_{CM}}{\partial P_{BO}} \\ \frac{\partial U_{INT}}{\partial P_{CO}} & \frac{\partial U_{INT}}{\partial P_{BO}} \end{bmatrix} \begin{bmatrix} \Delta P_{CO} \\ \Delta P_{BO} \end{bmatrix} + \begin{bmatrix} \frac{\partial U_{CM}}{\partial U_{CO}} & \mathbf{0} \\ \frac{\partial U_{INT}}{\partial U_{CO}} & \mathbf{0} \end{bmatrix} \begin{bmatrix} \Delta U_{CO} \\ \mathbf{0} \end{bmatrix} \\ \begin{bmatrix} \frac{\partial U_{CM}}{\partial P_{CO}} & \frac{\partial U_{CM}}{\partial P_{BO}} \\ \frac{\partial U_{INT}}{\partial P_{CO}} & \frac{\partial U_{INT}}{\partial P_{BO}} \end{bmatrix} = \left\{ \begin{bmatrix} \mathit{diag}(k) & \mathbf{0} \\ \mathbf{0} & \mathbf{0} \end{bmatrix} + \begin{bmatrix} J_{m/m} & J_{m/n} \\ J_{n/m} & J_{n/n} \end{bmatrix} \right\}^{-1} \times \begin{bmatrix} \mathit{diag}(1) & \mathbf{0} \\ \mathbf{0} & \mathit{diag}(\varepsilon)^{(t)} \end{bmatrix} \\ \begin{bmatrix} \frac{\partial P_{CM}}{\partial U_{CO}} & \mathbf{0} \\ \frac{\partial P_{INT}}{\partial U_{CO}} & \mathbf{0} \end{bmatrix} = \left\{ \begin{bmatrix} J_{m/m} & J_{m/n} \\ J_{n/m} & J_{n/n} \end{bmatrix}^{-1} + \begin{bmatrix} \mathit{diag}(k) & \mathbf{0} \\ \mathbf{0} & \mathbf{0} \end{bmatrix} \right\}^{-1} \times \begin{bmatrix} \mathit{diag}(k) & \mathbf{0} \\ \mathbf{0} & \mathbf{0} \end{bmatrix} \end{cases} \quad (12)$$

inverters which equals to the total available wind power subtracted by the power curtailment $\sum_1^S (P_{wf,f} - P_{cur,f})$, total line losses $\sum_1^V P_{loss}$ and the power loss of the inserted resistance of VRs $\sum_1^I P_{INT,VR}$ (if only VRs are in use).

4.2 Constraints

Analogue to the AC system practice, the operation of a DC grid is subjected to both equality constraints and inequality constraints. These constraints are listed below (i.e. (14)–(16))

4.2.1 Power flow equality constraints: The power is balanced amongst a converter at a node (e.g. i) and connected DC branches:

$$P_{CM,i} - P_{T,i} = 0 \quad (14)$$

where $P_{T,i}$ is the total power transmitted through connected DC branches.

4.2.2 DC system inequality constraints: DC system inequality constraints include the physical power constraints of converters, voltage constraints of converters and power constraints of DC branches

$$\begin{cases} P_{CM,i}^{\min} \leq P_{CM,i} \leq P_{CM,i}^{\max} \\ U_{CM,i}^{\min} \leq U_{CM,i} \leq U_{CM,i}^{\max} \\ P_{BR,i}^{\min} \leq P_{BR,i} \leq P_{BR,i}^{\max} \end{cases} \quad (15)$$

The minimum physical power constraints $P_{CM,i}^{\min}$ is the negative form of $P_{CM,i}^{\max}$, indicating the constraints for bidirectional power flow.

4.2.3 Control inequality constraints: The boundaries of control orders setting are given as

$$\begin{cases} P_{CO,i}^{\min} \leq P_{CO,i} \leq P_{CO,i}^{\max} \\ U_{CO,i}^{\min} \leq U_{CO,i} \leq U_{CO,i}^{\max} \\ P_{BO,i}^{\min} \leq P_{BO,i} \leq P_{BO,i}^{\max} \end{cases} \quad (16)$$

Note that, the voltage/power droop for converter control could be less changed compared with other control orders and thus in this study the droop characteristics are assumed to be unchanged.

4.3 Optimisation method

The modelling of optimisation is based on an OPF-Newton approach. This algorithm has been tested in practical AC systems [23, 24] and validated to be very efficient. The basic idea is well-established in these references while modification has been made to fit this study of coordinating the control of active DC components to optimise wind power delivery. Briefly, the power flow equality constraints (i.e. a set of (14)) can be extended using the power flow matrix developed in Section 3 as

$$\begin{bmatrix} \text{diag}(1) & \mathbf{0} \\ \mathbf{0} & \text{diag}(\epsilon)^{(t)} \end{bmatrix} \begin{bmatrix} P_{CO} \\ P_{BO} \end{bmatrix} + \begin{bmatrix} \text{diag}(k) & \mathbf{0} \\ \mathbf{0} & \mathbf{0} \end{bmatrix} \left\{ \begin{bmatrix} U_{CO} \\ \mathbf{0} \end{bmatrix} - \begin{bmatrix} U_{CM} \\ \mathbf{0} \end{bmatrix} \right\} - \begin{bmatrix} U_{CM} \\ U_{INT} \end{bmatrix} \otimes \begin{bmatrix} G & G_c^T \\ G_c & \mathbf{0} \end{bmatrix} \begin{bmatrix} U_{CM} \\ U_{INT} \end{bmatrix} = \mathbf{0} \quad (17)$$

The state variables of DC grid (e.g. measured voltage and power) are

represented by a vector \mathbf{x} while controllable variables (e.g. voltage orders and power orders) are denoted as vector \mathbf{u} . The inequality constraints in (15)–(16) are then modified as

$$\mathbf{h}(\mathbf{x}, \mathbf{u}) \leq \mathbf{b} \quad (18)$$

$$\mathbf{h}(\mathbf{x}, \mathbf{u}) = \begin{bmatrix} P_{BO,i} \\ P_{CM,i} \\ U_{CM,i} \\ I_{BR,i} \\ P_{CO,i} \\ U_{CO,i} \\ -P_{BO,i} \\ -P_{CM,i} \\ -U_{CM,i} \\ -P_{BR,i} \\ -P_{CO,i} \\ -U_{CO,i} \end{bmatrix}, \quad \mathbf{b} = \begin{bmatrix} P_{BO,i}^{\max} \\ P_{CM,i}^{\max} \\ U_{CM,i}^{\max} \\ I_{BR,i}^{\max} \\ P_{CO,i}^{\max} \\ U_{CO,i}^{\max} \\ -P_{BO,i}^{\min} \\ -P_{CM,i}^{\min} \\ -U_{CM,i}^{\min} \\ -P_{BR,i}^{\min} \\ -P_{CO,i}^{\min} \\ -U_{CO,i}^{\min} \end{bmatrix} \quad (19)$$

The objective function, equality constraints and inequality constraints are all specified. The linearised equations developed in Section 3 can then be used to solve the following optimisation problem (see (20))

The maximisation of wind power delivery can be achieved by re-dispatching optimised control orders of converters and DC-PFCs. A flow chart of optimisation is presented in Fig. 6. The optimisation starts with the specification of DC system topology (e.g. numbers of DC devices, connections). This is followed by the initialisation of control orders and system conductance. After the initialisation, the expression of power flow needs to be linearised before solving the equality constraints. The progress of solving the equality constraints then takes a few iterations until the error between P_{CM} and P_T is smaller than a defined value (i.e. ζ). Note that well-designed initialisation could avoid the need of iterations. The outputs are the updated vectors $\mathbf{h}(\mathbf{x}, \mathbf{u})$ and linearised matrix $(\partial \mathbf{h}(\mathbf{x}, \mathbf{u}) / \partial \mathbf{u})$. The required amount of change in the vector of control orders (i.e. $\Delta \mathbf{u}$) can then be estimated. An additional step is included to re-assess all the constraints with the updated control orders. If the error between the previous results and the new iteration is less than a defined value (i.e. $\Delta \mathbf{u}^{(i+1)} - \Delta \mathbf{u}^{(i)} < \mu$), a precise vector of control orders will eventually be obtained and output for the maximisation of wind power delivery.

5 Case study

The effectiveness of coordinating control of DC devices on optimising the wind power is validated on a 9-port DC system integrated with one CVS (Fig. 7). This system has a DC voltage rate of ± 400 kV. The delivery of wind power is through four offshore converters which can effectively be considered as in power control mode. However, the equivalences of ‘power orders’ are naturally determined by the offshore wind conditions. These offshore converters will import all the generated wind power to the DC system if the power does not reach the physical rate of any DC branch or converter. Conversely, in the events of overloading, the wind farms will have to reduce the generation which leads to the curtailment of wind power.

$$\begin{aligned} & \text{Max} && \left\{ \sum_1^r P_{inv,i} \right\} \\ & \text{s.t.} && \begin{bmatrix} \text{diag}(1) & \mathbf{0} \\ \mathbf{0} & \text{diag}(\epsilon)^{(t)} \end{bmatrix} \begin{bmatrix} P_{CO} \\ P_{BO} \end{bmatrix} + \begin{bmatrix} \text{diag}(k) & \mathbf{0} \\ \mathbf{0} & \mathbf{0} \end{bmatrix} \left\{ \begin{bmatrix} U_{CO} \\ \mathbf{0} \end{bmatrix} - \begin{bmatrix} U_{CM} \\ \mathbf{0} \end{bmatrix} \right\} - \begin{bmatrix} U_{CM} \\ U_{INT} \end{bmatrix} \otimes \begin{bmatrix} G & G_c^T \\ G_c & \mathbf{0} \end{bmatrix} \begin{bmatrix} U_{CM} \\ U_{INT} \end{bmatrix} = \mathbf{0} \\ & && \mathbf{h}(\mathbf{x}, \mathbf{u}) \leq \mathbf{b} \end{aligned} \quad (20)$$

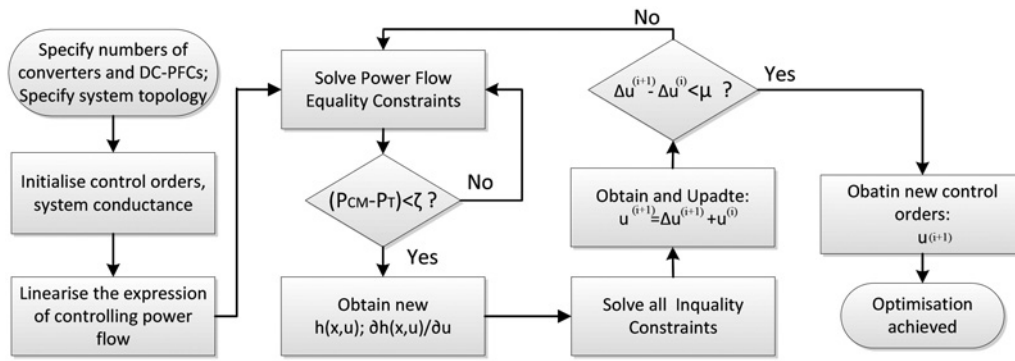


Fig. 6 Flow chart of solving OPF based on modified OPF-Newton approach

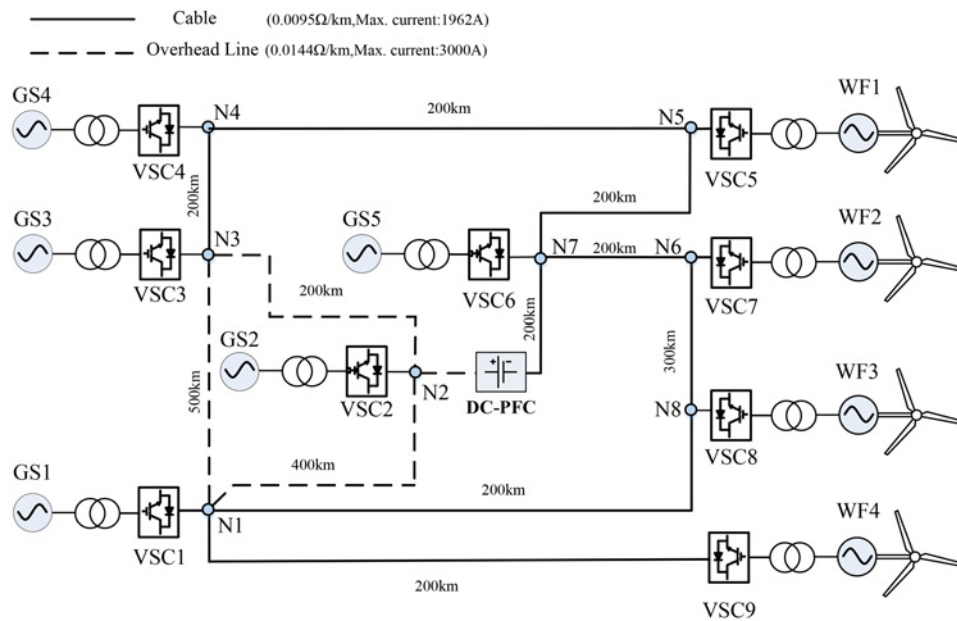


Fig. 7 9-port DC system with the integration of a DC-PFC

On the receiving end are four onshore rectifiers with DC voltage droop control. Converters VSC1–VSC4 are connected to strong AC system thus share the responsibility of regulating DC voltage. Another converter VSC5 is assumed to be connected with a weak AC system and thus consistently in power control mode.

A CVS is located at node N2 to avoid overloading of a DC branch (i.e. initially controls the power of Link N2–N7) and coordinate with converters on optimising the power delivery.

The initial control setting and physical rate of controllable DC devices are given in Table 1. The sign convention of power in this paper is defined as:

1. Import power to DC Grid: Positive (+).
2. Export power from DC Grid: Negative (–).

5.1 Case one – re-dispatching of control orders

Case one aims to show the effectiveness of re-dispatching control order on reducing power losses. The generation of wind power is very low and thus there is no occurrence of overloading. The results are given as Table 2 which shows the change of control orders for different DC devices. Since the power generation is low, the optimisation results show a rise of DC voltage which means the GDC aims to raise the DC voltage and thus reduce power losses. Meanwhile, the import onshore converter VSC1 increases its power order, tending to inject more power into the DC grid while the export converter VSC2 and VSC4 reduce the

power demand. Note that VSC5 is connected with weak system and thus its power order stays unchanged. The DC-PFC inserts a series voltage of –3.901 kV which leads to a power of 3.3 MW extracted from its DC side to its AC side. (As CVS is used, the power of 3.3 MW will not be dissipated.) The power loss of this

Table 1 Parameters of DC devices

DC device	Rate of device	Control mode	Control setting
VSC1	±420 kV; 2400 MW	voltage droop control	$P_{CO} = 1500$ MW; $V_{CO} = 818.17$ kV; $k = -60$ MW/kV
VSC2	±420 kV; 2400 MW	voltage droop control	$P_{CO} = -1900$ MW; $V_{CO} = 809.54$ kV; $k = -100$ MW/kV
VSC3	±420 kV; 2400 MW	DC voltage control	$V_{CO} = 800$ kV
VSC4	±420 kV; 1200 MW	voltage droop control	$P_{CO} = -800$ MW; $V_{CO} = 802.17$ kV; $k = -60$ MW/kV
VSC5	±420 kV; 200 MW	converter power control	$P_{CO} = -100$ MW
VSC6	±420 kV; 2400 MW	effective power control	$P_{CO} = 400$ MW
VSC7	±420 kV; 2400 MW	effective power control	$P_{CO} = 500$ MW
VSC8	±420 kV; 1500 MW	effective power control	$P_{CO} = 200$ MW
VSC9	±420 kV; 1500 MW	effective power control	$P_{CO} = 200$ MW
DC-PFC	±15 kV	branch power control	$P_{Bo} = -463.4$ MW (inserted zero voltage)

Table 2 Change of control orders in *Case one*

DC device	Change of power orders (ΔP_{CO} , ΔP_{BO})	Change of voltage orders (ΔU_{CO}), kV
VSC1	+369.2 MW	+20.43
VSC2	+542.6 MW	+18.78
VSC3	–	+24.13
VSC4	+92.0 MW	+22.26
DC-PFC	–48.3 MW (inserted –3.901 kV)	–

Table 3 Comparison in *Case one*

Items	Order unchanged, MW	Order Re-dispatched, MW	Power difference, MW
available wind power	1300	1300	0
power generation	1300	1300	0
power curtailment	0	0	0
line loss	32.76	18.49	–14.27
wind power received	1175.5	1281.51	14.27

Table 4 Change of control orders in *Case two*

DC device	Change of power orders (ΔP_{CO} , ΔP_{BO})	Change of voltage orders (ΔU_{CO}), kV
VSC1	–665.3 MW	+6.621
VSC2	–5.69 MW	+5.222
VSC3	–	+6.780
VSC4	–400.0 MW	+7.303
DC-PFC	+77.8 MW (inserted +3.525 kV)	–

CVS is only 0.0243 MW which is much smaller than its power exchange between the DC side and the AC side.

A comparison has been made in Table 3. It can be found with the re-dispatched control order, the line losses are reduced by 14.27 MW (i.e. 1.41% of the generated power). The benefits brought by using the optimisation are apparently shown.

5.2 Case two – increase of wind generation

Case two aims to show the performance of optimisation in an event of increased wind generation. The generation of wind power is assumed to be $P_{WF4} = 1500$ MW; $P_{WF3} = 1700$ MW; $P_{WF2} = 1800$ MW and $P_{WF1} = 2200$ MW. By applying the same method, the optimised results are obtained and shown in Tables 4 and 5. The power generation is massively increased compared with that in *Case One*. Therefore, the onshore converters tend to export more power by increasing their power demand (i.e. modulus of power

Table 5 Comparison in *Case two*

Items	Order unchanged, MW	Order Re-dispatched, MW	Power difference, MW
available wind power	7200	7200	0
power generation	4801.7	5299.4	497.7
power curtailment	2398.3	1900.6	–497.7
line loss	162.17	152.26	–9.91
wind power received	4659.4	5147.14	507.61

Table 6 Comparison in *Case three*

Items	Order unchanged	Order keeps updated	Power difference
available wind power	266.9 GW (1 p.u)	266.9 GW (1 p.u)	0 GW
power generation	0.8699 p.u	0.9242 p.u	0.0543 p.u
power curtailment	0.1301 p.u	0.0758 p.u	–0.0543 p.u
line loss	0.0272 p.u	0.0159 p.u	–0.0113 p.u
wind power received	224.92 GW (0.843 p.u)	242.43 GW (0.908 p.u)	17.51 GW (0.065 p.u)

order for exporting). The voltage orders slightly rise until voltage at Node 5 (linked with VSC5) reaches the voltage limit. The comparison of performance of using initial control order and re-dispatched control order is shown in Table 5. Power curtailment occurs in both events due to the overloading of Link N4–N5 (algorithm for power curtailment is introduced in [25] and out of the scope of this paper). However, with the re-dispatched control order, the DC-PFC aims to deliver +77.8 MW more power through Link N2–N7 and the voltage of VSC4 tends to rise to mitigate the overloading. This results in the reduction of power curtailment by 497.7 MW. Moreover, the use of the re-dispatched control orders also leads to smaller line losses though there is more power delivered within DC branches. The total power received is increased by 507.61 MW.

5.3 Case three – long term simulation

Case three aims to show the benefits of coordinating control of the DC-PFC and converters in a long term. The simulation length is set to 168 h (i.e. one week) for this case. The wind power generation keeps varying with a low wind load factor (e.g. average wind speed is 6.3 m/s) and the control orders will keep being optimised according to the change of amount of generated power. The modelling of wind power generation is Monte-Carlo-based and the details are given in the Appendix.

The results are shown in Table 6. It shows that by updating control orders, the power curtailment and line losses are reduced by 0.0543 and 0.0113 p.u correspondingly. An extra of 17.51 GW power has been received by the onshore system.

6 Conclusion

This paper has proposed to coordinate the control of AC/DC converters and DC-PFCs thus to optimise the power flow within a DC grid. An analytical expression is derived to quantise the impact of changing control orders on system power flow. Method for optimising power flow has been developed based on an OPF-Newton approach. The effectiveness of proposed methods has been demonstrated by three case studies with different conditions of wind generation. Results show that by the re-dispatching of optimised control orders, both the curtailment of wind power and the line losses are significantly reduced.

7 Acknowledgments

Jingli Guo's work was supported by the National Natural Science Foundation of China under grant 51261130471. Chuanyue Li's work was supported by China Scholarship Council under the project 201408060016. Jun's work was supported by Enhanced Renewable Integration through Flexible Transmission Options (ERIFT) programme under Grant EP/K006312/1. Information on how to access all data supporting the results in this article can be found at Cardiff University data catalogue at: <http://dx.doi.org/10.17035/d.2016.0008122492>.

8 References

- 1 Bresesti, P., Kling, W.L., Hendriks, R.L., *et al.*: 'HVDC connection of offshore wind farms to the transmission system', *IEEE Trans. Energy Convers.*, 2007, **22**, (1), pp. 37–43
- 2 Giddani, O., Adam, G.P., Anaya-Lara, O., *et al.*: 'Grid integration of offshore wind farms using multi-terminal DC transmission systems (MTDC)'. 5th IET Int. Conf. Power Electronics Machines Drives, 2010, pp. 1–6
- 3 Henry, S., Denis, A.M., Panciatici, P.: 'Feasibility study of off-shore HVDC grids'. IEEE PES General Meeting, 2010, pp. 1–5
- 4 Wijk, U., Lindgren, J., Winther, J., *et al.*: 'Dolwin1-Further achievements in HVDC offshore connections'. EWEA Offshore 2013, Frankfurt, Germany, November 2013, pp. 1–6
- 5 Johannesson, K., Gustafsson, A., Karlstrand, J., *et al.*: 'Light cables for long distance grid connection'. European Offshore Wind Conf., Stockholm, Sweden, September 2009, pp. 1–5
- 6 Jiang, X., Jiang, Y., Yin, Y., *et al.*: 'A demonstration project of flexible DC power transmission in shanghai nanhui wind power station', *High Volt. Eng.*, 2015, **41**, (4), pp. 1132–1139
- 7 Gomis-Bellmunt, O., Liang, J., Ekanayake, J., *et al.*: 'Topologies of multiterminal HVDC-VSC transmission for large offshore wind farms', *Electr. Power Syst. Res.*, 2011, **81**, (2), pp. 271–281
- 8 Veilleux, É., Ooi, B.T.: 'Multi-terminal HVDC grid with power flow controllability'. CIGRE, 2012
- 9 Deng, N., Zhang, X.P., Wang, P.Y., *et al.*: 'A DC current flow controller for meshed modular multilevel converter multiterminal HVDC grids', *CSEE J. Power Energy Syst.*, 2015, **1**, (1), pp. 43–51
- 10 Jovic, D., Hajian, M., Zhang, H., *et al.*: 'Power flow control in DC transmission grids using mechanical and semiconductor based DC/DC devices'. 10th IET Int. Conf. AC DC Power Transmission, 2012, pp. 1–6
- 11 Mu, Q., Liang, J., Li, Y., *et al.*: 'Power flow control devices in DC grids'. IEEE PES General Meeting, 2012, pp. 1–5
- 12 Xu, L., Yao, L.: 'DC voltage control and power dispatch of a multi-terminal HVDC system for integrating large offshore wind farms', *IET Renew. Power Gener.*, 2011, **5**, (3), pp. 223–233
- 13 Liang, J., Jing, T., Gomis-Bellmunt, O., *et al.*: 'Operation and control of multiterminal HVDC transmission for offshore wind farms', *IEEE Trans. Power Deliv.*, 2007, **26**, (4), pp. 2596–2604
- 14 Barker, C.D., Whitehouse, R.: 'Autonomous converter control in a multi-terminal HVDC system'. IET Int. Conf. on AC and DC Power, London, 2010, pp. 1–5
- 15 Barker, C.D., Whitehouse, R.: 'Further Developments in autonomous converter control in a multi-terminal HVDC system'. IET Int. Conf. on AC and DC Power, Birmingham, 2012, pp. 1–6
- 16 Barker, C.D., Whitehouse, R., Wang, S., *et al.*: 'Risk of multiple cross-over of control characteristics in multi-terminal HVDC'. IET Int. Conf. on AC and DC Power, Birmingham, UK, February 2015, pp. 1–7
- 17 Barker, C.D., Whitehouse: 'A current flow controller for use in HVDC grids'. IET Int. Conf. on AC and DC Power, Birmingham, 2012, pp. 1–6
- 18 Chen, W., Zhu, X., Yao, L., *et al.*: 'An interline DC power-flow controller (IDCPF) for multiterminal HVDC system', *IEEE Trans. Power Deliv.*, 2015, **30**, (4), pp. 2027–2036
- 19 Barker, C.D., Whitehouse, R.: 'Current flow controller'. US Patent Application, 2015/0180231 A1, 2015
- 20 Veilleux, E., Ooi, B.-T.: 'Multiterminal HVDC with thyristor power-flow controller', *IEEE Trans. Power Deliv.*, 2012, **27**, (3), pp. 1205–1212
- 21 Balasubramaniam, S., Liang, J., Ugalde-Loo, C.E.: 'Control, dynamics and operation of a dual H-bridge current flow controller'. Energy Conversion Congress and Exposition (ECCE), Montreal, September 2015, pp. 2386–2393
- 22 Wang, S., Barker, C.D., Whitehouse, R., *et al.*: 'Experimental validation of autonomous converter control in a HVDC grid'. European Conf. on Power Electronics and Application, Lappeenranta, August 2014, pp. 1–10
- 23 Sun, D.I., Ashley, B., Brewer, B., *et al.*: 'Optimal power flow by Newton approach', *IEEE Trans. Power Appl. Syst.*, 1984, **103**, (10), pp. 2864–2880
- 24 Maria, G.A., Findlay, J.A.: 'A Newton optimal power flow program for Ontario Hydro EMS', *IEEE Trans. Power Syst.*, 1978, **2**, (3), pp. 576–584
- 25 Wang, S., Liang, J., Wen, A., *et al.*: 'Cost and benefits analysis of VSC-HVDC schemes for offshore wind power transmission', *Autom. Electr. Power Syst.*, 2014, **37**, (4), pp. 36–43

9 Appendix

For *Case three*, the wind power generation is modelled as follows. The Weibull law is used to model the wind speed

$$\begin{cases} f(W, A, B) = \frac{B}{A} W^{B-1} \times e^{-(W/A)^B} \\ F(W, A, B) = 1 - e^{-(W/A)^B} \end{cases} \quad (21)$$

where A is the scale parameter; B is the shape parameter; W is the wind speed; $f(W, A, B)$ is the probability density function of wind speed, and $F(W, A, B)$ is the cumulative distribution function. The hourly power generation from one wind farm based on different wind speeds can be expressed as

$$P(W) = \begin{cases} 0 & 0 < W < W_{\text{cut_in}} \\ \frac{1}{2} S \times \rho \times W^3 \times C_p \times n & W_{\text{cut_in}} \leq W < W_{\text{rated}} \\ P_{\text{rated}} & W_{\text{rated}} \leq W < W_{\text{cut_off}} \\ 0 & W_{\text{cut_off}} \leq W \end{cases} \quad (22)$$

where S is the swept area of turbine blade; ρ is the air density; P_{rated} is the rated power; C_p is the power coefficient; n is the number of wind turbines in a wind farm; $W_{\text{cut_in}}$, W_{rated} and $W_{\text{cut_off}}$ are cut-in speed, rated speed and cut-off speed accordingly. In offshore area, the power generation between two wind farms is expected to have a high cross-correlation, which can be represented by

$$R_{x,y} = \frac{(1/N) \sum_{i=1}^N (P_{xi} - \mu_x)(P_{yi} - \mu_y)}{\sigma_x \sigma_y} \quad (23)$$

where P_{xi} and P_{yi} are the output power from wind farm X and Y at time i ; μ_x and μ_y are the mean value of power output while σ_x and σ_y are the standard deviations. All the parameter for the modelling is given as Table 7.

Table 7 Parameter for modelling the generation of wind power

Scale parameter (A)	11.12																
Shape parameter (B)	2.25																
Average/mean speed of Wind (μ)	6.3 m/s																
Standard deviations of Wind (σ)	21.45																
Rated speed of wind (W_{rated})	13 m/s																
Cut in speed of wind ($W_{\text{cut_in}}$)	3.5 m/s																
Cut off speed of wind ($W_{\text{cut_off}}$)	25 m/s																
Number of wind turbines in each wind farm (n)	400																
Rated power of each wind farm (P_{rated})	2400 MW																
Swept area of turbine blade(S)	12,469 m ²																
Air density (ρ)	1.225 kg/m ³																
Cross-correlation ($R_{x,y}$) (WF1, WF2, WF3 and WF4)	<table border="1" style="display: inline-table; vertical-align: middle;"> <tbody> <tr> <td>1.0000</td> <td>0.9618</td> <td>0.8906</td> <td>0.8525</td> </tr> <tr> <td>0.9618</td> <td>1.0000</td> <td>0.8696</td> <td>0.8377</td> </tr> <tr> <td>0.8906</td> <td>0.8696</td> <td>1.0000</td> <td>0.8551</td> </tr> <tr> <td>0.8525</td> <td>0.8377</td> <td>0.8551</td> <td>1.0000</td> </tr> </tbody> </table>	1.0000	0.9618	0.8906	0.8525	0.9618	1.0000	0.8696	0.8377	0.8906	0.8696	1.0000	0.8551	0.8525	0.8377	0.8551	1.0000
1.0000	0.9618	0.8906	0.8525														
0.9618	1.0000	0.8696	0.8377														
0.8906	0.8696	1.0000	0.8551														
0.8525	0.8377	0.8551	1.0000														